Characterization of Candidate Materials for Remote Recession Measurements of Ablative Heat Shield Materials

Bradley D. Butler [*], **Michael Winter**[†], **Francesco Panerai**[‡],
Alexandre Martin[§], **Sean C.C. Bailey**[**]
University of Kentucky, Department of Mechanical Engineering, Lexington, KY 40506-0503, USA

Margaret Stackpoole [††]
NASA Ames Research Center, Moffett Field, CA 94035-1000, USA

Paul M. Danehy [‡‡] **, Scott Splinter** [§§]
NASA Langley Research Center, Hampton, VA 23681-2199, USA

A method of remotely measuring surface recession of a material sample in a plasma flow through emission spectroscopy of the post shock layer was characterized through experiments in the NASA Langley HYMETS arcjet facility. Different methods for delivering the seed products into the Phenolic Impregnated Carbon Ablator (PICA) material samples were investigated. Three samples were produced by seeding the PICA material with combinations of Al, Si, HfO_2, VB_2, Al_2O_3, SiO_2, TiC, HfC, NaCl, and $MgCl_2$ through infusing seed materials into a core of PICA, or through encapsulating seed material in an epoxy disk, mechanically bonding the disk to a PICA sample. The PICA samples seeded with the candidate tracers were then tested at surface temperatures near 2400 K under low pressure air plasma. The emission of Al, Ti, V, Na, and Mg in the post-shock layer was observed in the UV with a high resolution imaging spectrometer viewing the whole stagnation line from the side, and from UV to NIR with a fiber-coupled miniaturized spectrometer observing the sample surface in the wavelength range from 200 nm to 1,100 nm from the front through a collimator. Al, Na, and Mg were found to be emitting in the post-shock spectra even before the recession reached the seeding depth - therefore possibly characterizing the pyrolysis process rather than the recession itself. The appearance of Ti and V emission in the spectra was well correlated with the actual recession which was monitored through a video of the front surface of the sample. The applicability of a seed material as an indicator for recession appears to be related to the melting temperature of the seed material. Future parametric studies will be carried out in low power plasma facilities at the University of Kentucky.

[*] PhD candidate, Department of Mechanical Engineering, 151 Ralph G. Anderson Building, Lexington, KY 40506-0503, USA, student member AIAA.
[†] Assistant Professor, Department of Mechanical Engineering, 185 Ralph G. Anderson Building, Lexington, KY-40506-0503, USA, Associate Fellow AIAA.
[‡] Research Fellow, Department of Mechanical Engineering, NASA Visiting Scientist, Thermal Protection, Materials Branch, member AIAA.
[§] Assistant Professor, Department of Mechanical Engineering, 261 Ralph G. Anderson Building, Lexington, KY-40506-0503, USA, Associate Fellow AIAA.
[**] Associate Professor, Department of Mechanical Engineering, 283 Ralph G. Anderson Building, Lexington, KY-40506-0503, USA, member AIAA.
[††] Senior Research Scientist, Thermal Protection Materials and Systems Branch, NASA Ames Research Center,
[‡‡] Research Scientist, Advanced Measurements and Data Systems Branch, MS 493. Associate Fellow AIAA.
[§§] Aerospace Engineer, Structural Mechanics and Concepts Branch, M/S 190, AIAA Member.

I. Introduction and Motivation

SPACECRAFT entering into a planet's atmosphere experience significant heat loads while the kinetic energy is dissipated during the slowing down of the vehicle. To protect the spacecraft, thermal protection systems (TPS) are needed. TPS can be divided in two categories: for lower entry speeds such as return from low earth orbit, radiative cooling may be sufficient and re-useable materials such as high temperature ceramics deliver sufficient performance. For higher entry speeds as experienced for re-entries from interplanetary missions, ablative materials are needed which thermally and mechanically decompose during the hot re-entry phase therefore dissipating additional energy to the surrounding gas.

The development of reliable TPS for atmospheric entries requires extensive material testing in ground test facilities under conditions relevant to high speed re-entry such as the NASA Ames arcjets. However, even these high power facilities are not capable of reproducing real flight conditions. Instead, an extrapolation of the ground test data to atmospheric entry conditions is necessary. This is achieved through aerothermochemistry simulation codes. Thus, aerothermochemistry and material response simulations have become the most important tool for designing new TPS systems.

Material recession and charring are two major processes determining the performance of ablative heat shield materials. For recession measurements during ground testing, optical methods such as imaging the sample surface during testing are under investigation[1] but require high alignment and instrumentation effort, therefore being not yet established as a standard measurement method. Typically, the characterization of recession relies widely on measurements of material thickness before and after testing, thus providing only information integrated over the test time. For char depth measurements, the most common method so far consists in investigation of sectioned samples after testing or in the case of capsule reentries such as Stardust where core extractions were performed to determine char information.[2] In flight, no reliable recession measurements are available, except total recession after recovering the heat shield on ground. Developments of electro-mechanical recession sensors have been started[3] but require substantial on board instrumentation adding mass and complexity. Motivated by the detection of tracer elements such as sodium, potassium, magnesium, and calcium in spectrally resolved data gathered during the airborne observation campaign of the Stardust sample return capsule,[4] a methodology for recession measurements through the detection of seed elements buried at known depths inside the TPS material was developed. A feasibility study in a NASA Ames arcjet facility was successfully conducted and showed promising results.[5] Applications besides ground testing are recession and possibly char depth measurements during actual re-entry. Detection through emission spectroscopy could be accomplished through ground based or airborne observation as performed during the Stardust[4] and Hayabusa[6] re-entries, through on-board spectrometers, or even through formation flight. However, an application of remote recession measurements to real missions requires further tests under controlled conditions to down-select the optimum seed materials and quantify the amounts needed and the achievable accuracy through this method before being proposed for a NASA mission.

The basic idea of remote recession sensing is to seed specific materials at a known depth inside the ablative material. Once recession reaches the seeding depth, the seed material comes in contact with the plasma, is gasified, and transported into the hot region of the post-shock layer by diffusion processes where the characteristic emission signatures can be detected by emission spectroscopy. The working principle is illustrated in Fig. 1. For detection, no spatial resolution of the optical system is needed as confirmed during the feasibility demonstration experiments at NASA Ames.[5] Spatial resolution through the thickness of the heat shield material, however, is achieved through a local deposition of the seed material in the TPS. The emission of the seed elements is then observed through external observation of the post shock plasma.

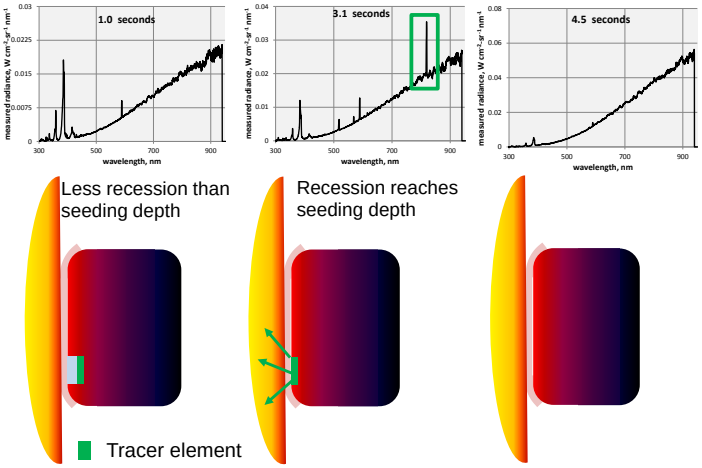

Figure 1. Illustration of remote recession sensing; spectra obtained during mArc testing.[5]

In preliminary experiments in a subscale developmental arcjet facility (mArc) at NASA Ames, the feasibility of this method was demonstrated by testing samples made of phenolic impregnated carbon ablator (PICA) which were

seeded with rods made of a polymer matrix which contained NaCl and $MgCl_2$.[5] The heat flux to the sample was measured to about 1,000 W/cm^2. The emission lines of magnesium and sodium were shown to be clearly visible on top of the thermal emission of the glowing sample. They appeared in the emission spectra at about 1.5 seconds after insertion and disappeared 3 seconds later as shown in Fig 2. A recession rate calculated from this time and the dimensions of the seed material was in good agreement with the value determined post-test from the total recession of the sample.

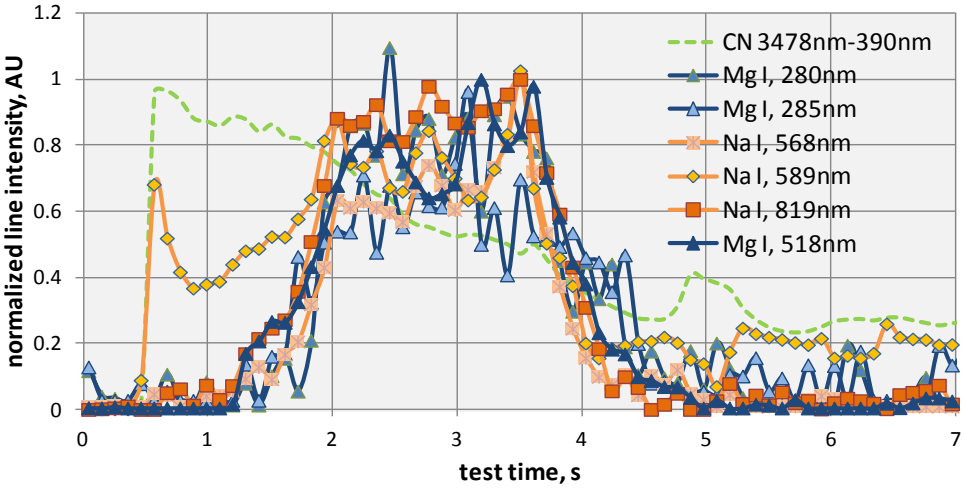

Figure 2. Time trace of normalized spectrally integrated line emission of sodium and magnesium during mArc testing vs. sample insertion time.[5]

While this previous experiment showed proof of concept of the technique, additional refinement is still needed. The method needs optimization such as signal intensity enhancement. Furthermore, more species need to be tested in order to allow measurements at multiple depths to be made remotely. This is the motivation for the current work. A method of delivery of the seed material to PICA samples was developed at NASA Ames, seed materials were selected, and three in-depth seeded samples were tested in the HYMETS facility[7,8] at NASA Langley. In the following, the strategy for delivering the seed materials into the PICA samples, the set-up used during HYMETS testing, and the results from these tests are described.

II. Seeding Methodology

Consideration has to be given to the selection of appropriate seed materials for remote recession sensing purposes. The physical properties of the chosen seed need to be suitable in the range of surface temperatures achieved during recession testing. If a materials melting or boiling temperature is too low it would likely evaporate and entrain with or interact with the pyrolysis gas generated by the phenolic material rather than indicate the recession process. The seed material must also be stable and non-reactive with either water or the PICA precursor solution. For an external observation during reentry, the spectral response characteristics of the seed material need to provide radiation which is visible on top of the thermal continuum emitted by the glowing surface at wavelengths above the absorption threshold of the atmosphere. The ideal particle size would be on the micron scale as a large surface area to volume ratio would help the phase transfer and spectral emission of the seed material in the post shock region. The materials used in this study represent suitable options that satisfy these requirements.

A. Delivery Methods

For a remote recession measurement method to provide useful information about the rate of recession, the location of the seed material relative to the receding surface and the extent of seed material need to be known as accurately as possible. Several methods of seed material delivery and placement were tested using FiberForm, the carbon fiber substrate of PICA. Delivery of the seed material with a solvent or epoxy as administered with a hypodermic needle proved to provide little control in how much of the FiberForm received the seed material.

A small amount of solvent or epoxy would wick through the porous material leaving no control on the size of the seeded region as seen in Figure 3. This result inspired the idea of infusing FiberForm with a seeded epoxy and machining it so a seed disk insert that could be placed at a defined location and depth in a TPS material. An extension of this method would be the creation of a seeded PICA material by incorporating the seed materials into the PICA manufacturing process.

Figure 3. FiberForm material where a seed material has been delivered with an epoxy resin which wicks through the material creating the darkened seeded region of uncontrollable size and quality.

The candidate materials must be tested to verify their compatibility with for the PICA infusion process. A selection criterion is the capability of seed particle to remain suspended in the PICA precursor material. Two tests were performed to characterize how well the seed particles would remain in suspension, the first being conducted in isopropanol. Samples were prepared by thoroughly mixing a nominal 0.5 g of seed material in a 20 ml vial of isopropanol. The samples were allowed to settle for three hours and afterwards the isopropanol with material in suspension was pulled off into a separate vial leaving the precipitate in the original vial. The isopropanol suspension was then placed under vacuum to aid evaporation, leaving just the material that had been in suspension. Al_2O_3 and HfO_2 performed the best out of the selected materials with more than 10% remaining in suspension compared to less than 2% in suspension as shown in Table 1.

Table 1. Percentage of candidate seed material which remains suspended in isopropanol after three hours of settling time.

Material	Suspension, %
Al_2O_3	56.46
HfO_2	12.83
VB_2	1.33
Al	1.06
SiC	0.81
TiO_2	0.80
ZrO_2	0.61
TaN	0.56

The top four seed materials for suspension in isopropanol, with the addition of silicon, were selected to be tested for suspension in the PICA precursor solution which is the material that is infused into the FiberForm in the making of PICA. The sample preparation followed that of the isopropanol tests with the exception of nominally 1 g of seed material being used. An additional test was conducted using magnesium chloride as the seed particle but the precursor solution reacted with ths seed material resulting in an unsuitable candidate.

To determine the amount of seed materials that remained in suspension, multiple density measurements of the seeded precursor were performed. The normalized results are shown in Figure 4.A slurry density formula was used to calculate the percentage of seed material remaining in suspension (compare Table 2). The suspension of candidate seed materials did not behave similarly between the precursor and isopropanol. An increase in suspension of Aluminum and VB_2 was seen with the precursor compared to isopropanol, while a decrease in suspension was seen with Al_2O_3 and HfO_2. Silicon was chosen to study how well it infuses throughout PICA with varying seed loads, since it had the largest particle size (44 micron) of the prior group.

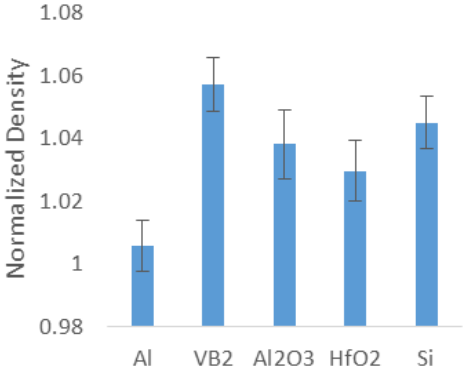

Figure 4. Normalized density of the PICA precursor solution with seed materials.

Table 2. Percentage of candidate seed material remaining suspended in the PICA precursor solution after three hours of settling.

Material	Suspension, %
Al	1.41
Al_2O_3	4.03
HfO_2	3.11
Si	4.72
VB_2	5.41

B. SEM Elemental Analysis of Seeded PICA

Four PICA samples were created following the standard PICA fabrication procedure except adding a high, medium, low, or no amount of silicon as a seed material to the precursor solution to determine the minimum loading required for a given volume. The low seed sample suffered damage to the edges of the sample during extraction rendering a density measurement and edge sampling impractical. The samples were weighed and then cleaved in two parts. The cleaved samples were analyzed using an energy dispersive X-ray spectroscopy (EDAX) to show the concentration and distribution of the Silicon seed material. The standard result for this type of analysis is an energy distribution, demonstrated for the high loading case and for the control case in Fig. 5. For the high loading case, there is a peak at the energy level corresponding to Silicon which is not present for the control case; indicating the silicon seed material was able to infuse throughout the PICA material.

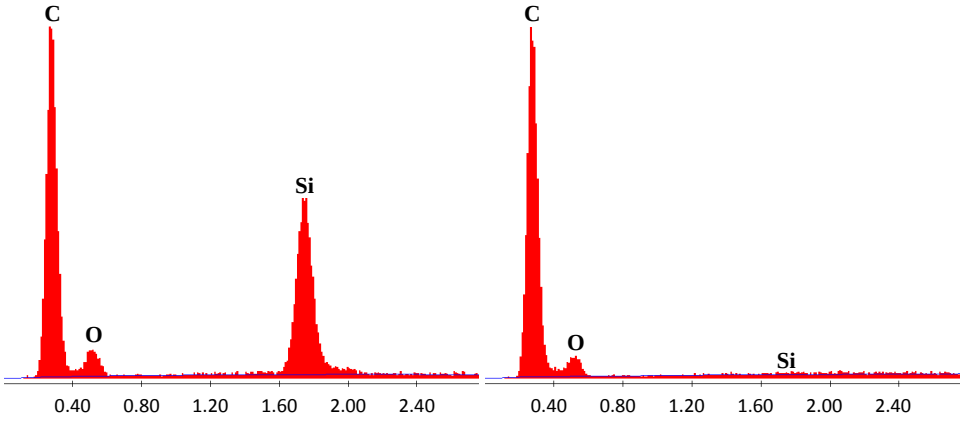

Figure 5. Left) EDAX response for the high loading of Silicon showing peaks corresponding to carbon, oxygen, and silicon. Right) EDAX response for the control sample showing a response only for carbon and oxygen.

Table 3. Details of the three Si load cases and the control PICA sample.

Loading	Mass of Si, g	Final Density, g/cc	Edge Si Concentration, %	Center Si Concentration, %
High	2.001	0.299	5.55	2.85
Medium	0.204	0.283	1.63	0.51
Low	0.034	-	-	0.09
Control	0.000	0.280	0.05	0.07

Elemental mapping and statistics were performed at the edge of the sample and then at the center to understand how effectively the seed particle is able to infuse through the FiberForm material along with the precursor solution as a carrier. The elemental mapping for the high silicon loading case is presented in Fig. 6 where the blue regions are the response from silicon. The concentration of seed was the highest at the edge of the PICA sample and decreased towards the center region showing that a gradient occurs, likely induced by the seed particle size. The small levels,

less than 0.10%, of silicon detected in the low loading and control samples are within the measurement uncertainty baseline of the machine and would indicate very minimal to no silicon seed in those two cases.

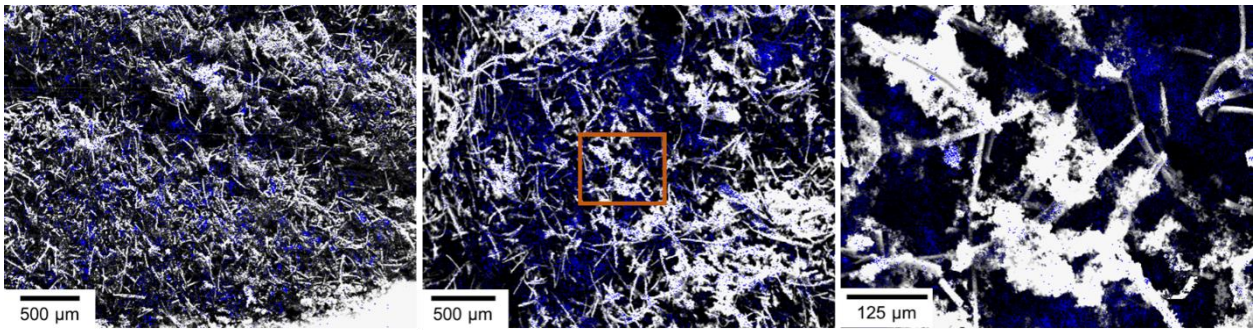

Figure 6. Elemental mapping of the high loading case showing the distribution of silicon at the a) edge, b) center, and c) center zoomed in area of b as denoted by the orange rectangle.

C. Test Sample Preparation

Two versions of seed infused PICA were produced to be used in arcjet test samples and for further characterization as listed in Table 4. Samples A and B were prepared by machining a core from the backside of a PICA sample and replacing it with a seeded PICA insert. This allows for recession to occur through about 1.7 mm of normal PICA before the seeded PICA is reached and will proceed to recess through a seeded section of PICA for the remaining duration of the test. A third test sample, designed to replicate the mArc tests, was created using an epoxy encapsulated seed disk of magnesium chloride and sodium chloride that was inserted into a segment of PICA machined from the back side and backed with a nominal PICA plug. Each of the samples was then inserted into a collar and affixed with RTV, as viewed in assembled state in Fig. 7. The RTV, comprised of silicon and iron oxide, is the red material seen on the surface of the sample between the collar and the PICA. A Li-2200 collar was used for protection from side heating but also forces the pyrolysis gasses to leave through the front of the sample. Li-220 is primarily composed consists primarily of SiO_2.

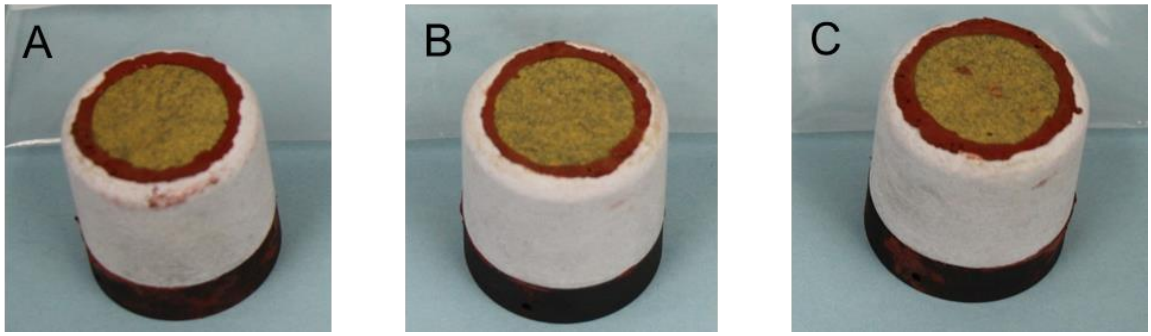

Figure 7. Final assembly of the three seeded PICA test samples. The red ring is RTV, the white collar encompasses the PICA sample and attaches it to the black graphite adapter for mounting in the HYMETS sample support system.

Table 4. Seed material type and amount for the seed infused PICA cores used in Samples A and B.

Sample A		Sample B	
Material	Amount, g	Material	Amount, g
Al	1.523	Al2O3	1.530
Si	1.599	SiO2	1.267
HfO2	1.517	HfC	1.561
VB2	1.522	TiC	1.547

III. Experimental Setups for HYMETS Testing

The NASA Langley HYMETS arcjet is one of the NASA ground test facilities for the experimental investigation of thermal protection materials. A 400 kW power supply is used to run a segmented-constrictor direct-current electric arc heater, which serves as the arc plasma generator. Test gasses are injected tangentially into the bore to produce a vortex flow, which spin-stabilizes the electric arc of the plasma generator. The heated mixture is then accelerated through a convergent-divergent 8-degree half-angle Mach 5 conical nozzle with a 12.7-mm diameter throat. To increase the footprint of the arc and thus protect the electrodes from rapid oxidation, argon (Ar) is injected near the anode. After passing through the test section, the flow exhausts into a 0.6-m diameter by 0.9-m long vacuum test chamber. A high capacity pumping system is used to evacuate the stagnated flow from the facility after being cooled. Depending on the tunnel conditions, the facility can be operated by a single technician, continuously, and for several hours.[7,8]

For the emission spectroscopy measurements, an Andor Shamrock spectrometer with 500 mm focal length in combination with a Princeton Instruments PIXIS:400BR_eXcelon CCD was used for spectral dispersion and detection. The spectrometer observed the stagnation region in front of the PICA samples through a side window of the HYMETS facility. The 150 lines/mm grating allowed for a simultaneous detection of a wavelength range from 204 nm to 550 nm with a spectral resolution of ~0.26 nm. A 445 mm focal length parabolic mirror and several redirecting mirrors were used to image a horizontal line onto the vertical entrance slit of the spectrometer. Since the sample position was not directly accessible through the side window, an additional periscope consisting of two mirrors under 45° tilt was placed inside the vacuum chamber to give a perpendicular line of sight onto the flow axis. In addition, a separate optical system, shown on the top right of Fig. 8, used a Thorlabs mirror collimator pointed at the sample front surface. This collimator imaged approximately the whole front surface of the sample. The signals were fed through an optical fiber to a Stellarnet Black Comet miniaturized spectrometer with a spectral range from 200 nm to 1,100 nm and a pixel resolution of 0.5 nm and time resolved spectra were taken over the insertion time of the sample. Figure 8 illustrates the emission spectroscopy setups and the viewing geometry inside the HYMETS chamber.

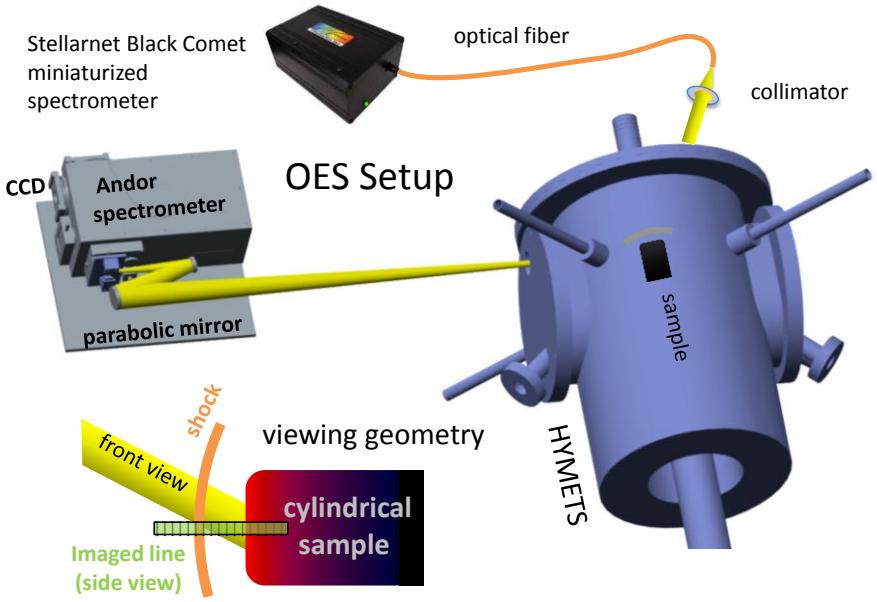

Figure 8. Setup for optical emission spectroscopy (OES) from the side with an Andor imaging spectrometer and from the front with a miniaturized fiber couples spectrometer and viewing geometry inside the HYMETS.

The CCD array height of 8 mm allowed for monitoring a line of 22 mm length inside the HYMETS facility. Focusing was done by imaging LEDs of different color on the camera with the grating tuned to zero order therefore producing an image without spectral resolution. Intensity calibration of both spectrometers was done through measuring the emission of a miniaturized spectral radiance source (Gigahertz-Optik BN-0102) calibrated between 300 nm and 1,100 nm and a deuterium lamp (Bentham CL3) calibrated to spectral irradiance between 200 nm and 400 nm. The irradiance values from the Deuterium lamp were used to obtain the spectral sensitivity in the UV and were scaled to the radiance values obtained from the Gigahertz lamp in the overlapping spectral region to achieve a calibration to spectral radiance over the entire measured spectrum.

IV. Experimental Data and Analysis

Three seeded samples were available for testing (A, B, and C). The method of delivery varied as described above, the seeding depth from the sample surface was roughly the same for all samples. Table 5 summarizes the sample configuration. All samples were tested at a condition with 300 SLM air as working gas, a stagnation pressure of 44 mbar, and a nominal cold wall heat flux of 200 W/cm^2 yielding sample surface temperatures between 3,800 and 3,900°F (2,366 and 2,422 K). For PICA samples without a collar, recession rates of about 0.1 mm/s were seen in earlier tests at that condition.

Table 5. Seeding information for the tested samples.

Sample	*Seeding method*	*Seed elements*	*Seeding Depth*
A	infused into a core of PICA	Al, Si, HfO_2, VB_2	1.76 mm
B	infused into a core of PICA	Al_2O_3, SiO_2, TiC, HfC	1.65 mm
C	encapsulated in an epoxy disk	NaCl, $MgCl_2$	1.69 mm

The high-resolution emission spectroscopy data from the side view was taken with an entrance slit width of 30 μm, and an acquisition time of 120 ms yielding a frame rate of 2.5 frames per second. In each frame the post shock region from shock to the sample surface (which is about 3 mm thick) is resolved with about 50 spectra showing spatial distribution of the observed radiation in this region. However, for the analysis of the seed elements, the temporal change contains the important information, i.e. when individual species show up in the measured spectra. Therefore, the spatial information in all spectra in each frame were summed up after being individually calibrated which corresponds to running the camera in full vertical binning mode, showing the total spectral emission of the entire post shock layer. The resulting spectra were plotted over time after sample insertion as shown in Fig. 9 for sample A, seeded with Al, Si, HfO_2, and VB_2, infused into a core of PICA.

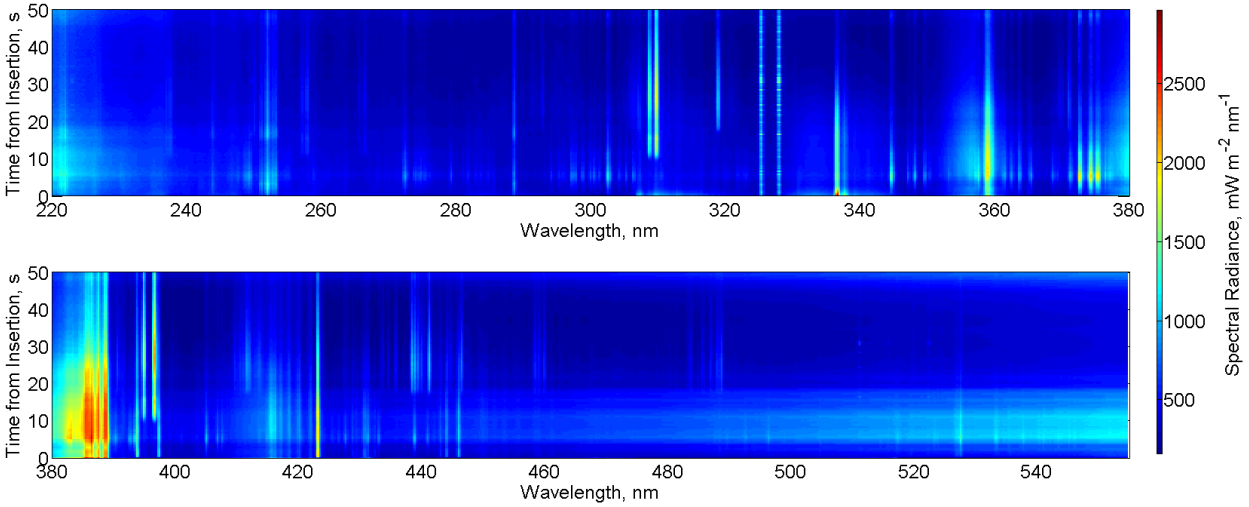

Figure 9. Time trace of integrated emission over the entire post-shock layer in front of sample A, seeded with Al, Si, HfO_2, and VB_2, infused into a core of PICA. Top: 220 nm to 380 nm, bottom: 380 nm to 555 nm.

The spectrum shown in the bottom-most row of Fig. 9 was taken right after sample insertion. The spectra evolve with test time towards the top of the figure. For the sake of clarity, the total wavelength range is split up in two regions from 220 nm to 380 nm (upper picture in Fig. 9) and from 380 nm to 555 nm (lower picture). The strong emission lines at 325 and 328 nm are from copper due to electrode erosion in the arcjet and are present in all spectra. Nearly all emission between 340 nm and 388 nm is likely to be from CN radiation, while the molecular bands near 336 nm are due to NH. Both can originate from plasma interactions with the silicon bond material RTV on the sample surface, with the collar material, and with pyrolysis products from PICA itself. The strong emission lines at 393, 397, and 423 nm are due to Ca and Ca^+ which is found in the carbon FiberForm itself.[9] Emission characteristic for the seed elements is seen from aluminum (Al) and vanadium (V). Strong Al lines are seen at 308, 310, 395, and 396 nm and appear at about 10 s after sample insertion. The strongest V lines are seen at 318 and 441 nm and appear after about 17 seconds, despite the fact that they were both seeded at the same location in the sample. Neither hafnium nor boron were identified in the spectra.

For the following analysis, the line integrals were built by summing all intensities of the corresponding line and subtracting an underlying trapezoid due to background emission (particularly important in wavelength regions with strong thermal continuum radiation). If normalized to their respective maxima, the time history of all aluminum lines followed the same profile, as did the individual vanadium lines. Representative for the other lines, the time history of the line intensities normalized to their respective maximum of Al at 310 nm and V at 318 nm are shown in Fig. 10. As an example for emission from samples without seed material, NH is added which starts emitting right after sample insertion.

The Al emission starts at about 10 s, has a peak at about 15 s, a local minimum at 19 s and a second peak after 30 s. The vanadium emission starts at about 17 s and follows qualitatively the time profile of the Al emission. If compared to images of the front surface of the sample during the test as shown in Fig 11, the seeded rod becomes visible on the front surface at about 17 s after insertion which agrees very well with the time the vanadium lines start being visible in the emission spectrum. Therefore the vanadium emission is interpreted as a suitable indicator for recession reaching the seeding depth. At 10 seconds when the aluminum emission starts to significantly increase, the recession has not yet reached the seeded part.

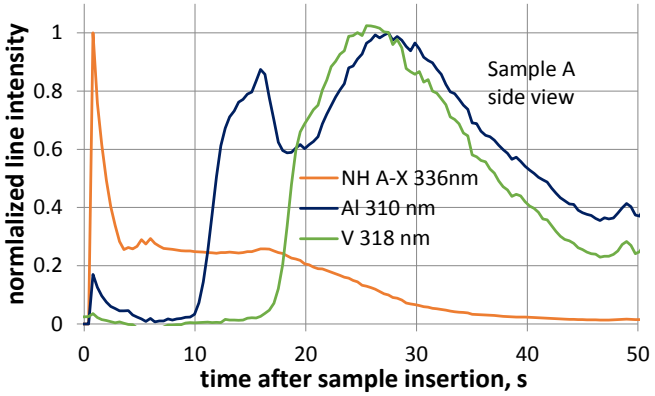

Figure 10. Line intensities of Al (310 nm), V (318 nm), and NH (336 nm) integrated over the entire post-shock layer in front of sample A vs. test time after sample insertion.

Although the collar material does contain some aluminum, the absence of Al lines in the spectra collected right after the injection, confirms than no contribution to the observed emission is due the collar.. Therefore, the Al emission is believed to be c ascribed to Al seeds transported by pyrolysis gases and blown into the boundary layer before recession reaches the seeding depth. As hypothesized, the radiation from the materials with lower melting and evaporation temperature indicates interactions with the pyrolysis gases rather than being an indicator for recession. Unfortunately, the seeded samples were not instrumented with in-depth thermocouples, otherwise the appearance of aluminum in the emission spectra could be linked to a temperature of the sample at the seeding depth at that time.

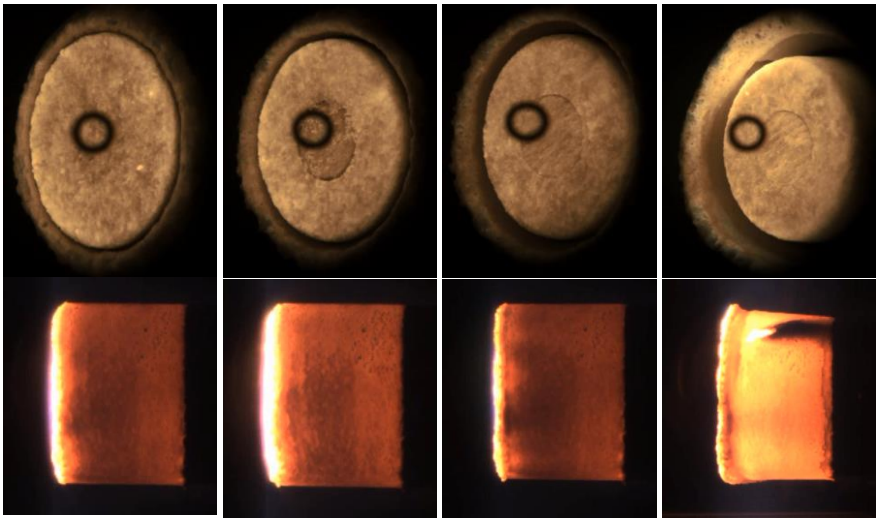

Figure 11. Front (top row) and side (bottom row) view of sample A at 10, 17, 30, and 59 seconds after sample insertion. (The black ring in the front view is a marker for the pyrometer measurement and no physical feature of the sample itself.)

The same procedure of calculating line intensities was performed for the front view spectra measured with the fiber-coupled miniaturized spectrometer. Due to the lower spectral resolution, and due to the large area of glowing

sample covered, the emission lines do not stand out as clearly as in the side view. However, line intensities could be extracted for aluminum and vanadium and show the same trends as seen in the side view, as illustrated in Fig. 12.

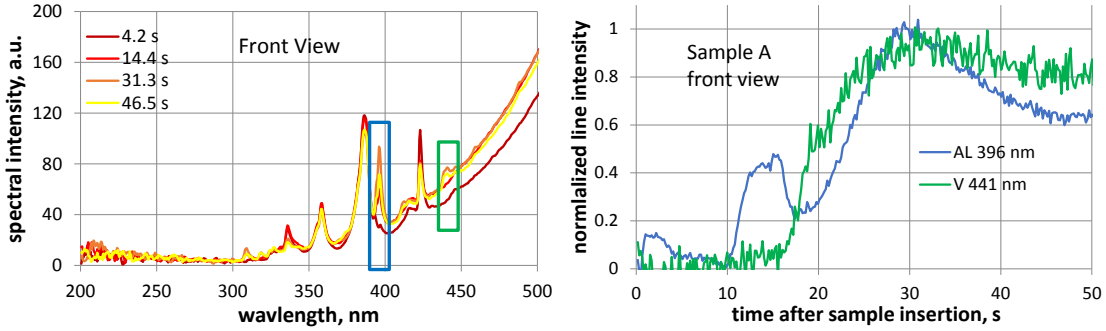

Figure 12. Front view spectra of sample A at increasing times after sample insertion (left) and line intensities for aluminum (emission line at 395 nm) and vanadium (emission line at 441 nm) (right).

Figure 13 shows FVB spectra for sample B, seeded with Al_2O_3, SiO_2, TiC, and HfC, infused into a core of PICA. As for Sample A, strong emission of copper, CN, calcium and NH is seen. The emission of seeded silicon cannot be separated from the silicon coming from the collar and is therefore not useful for recession measurements. The same is valid for carbon which is part of PICA itself. Again, hafnium could not be identified in the spectra.

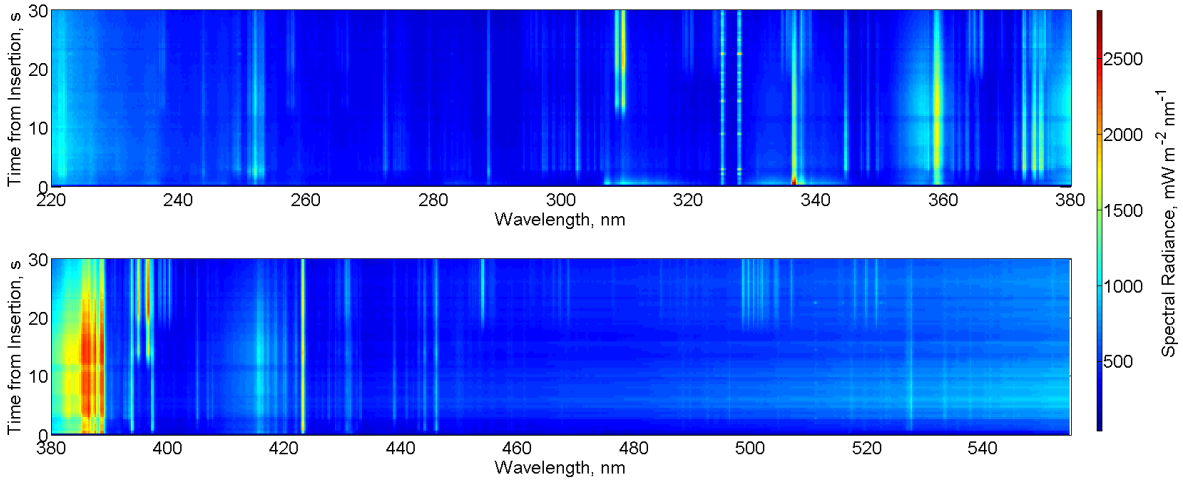

Figure 13. Time trace of integrated emission over the entire post-shock layer in front of sample B, seeded with Al_2O_3, SiO_2, TiC, and HfC, infused into a core of PICA.

However, the emission of aluminum (308, 310, 395, and 396 nm) and titanium (366, 399, and 453 nm and groups of lines around 500 and 519 nm) can be clearly observed. As seen for sample A, the Al lines appear in the spectrum at about 10 seconds after sample insertion and show a local maximum at 14 s. The titanium lines appear at about 17 s and peak at 25 s. These times correlate very well with the aluminum and vanadium emission in the test of sample A. Consequently, it is concluded that the Ti emission indicates that recession reached the seeding depth. Examples for the time trace of line intensities (Al at 310 and 396 nm, Ti at 453 nm and group around 500 nm) are shown in Fig. 14 to illustrate this behavior.

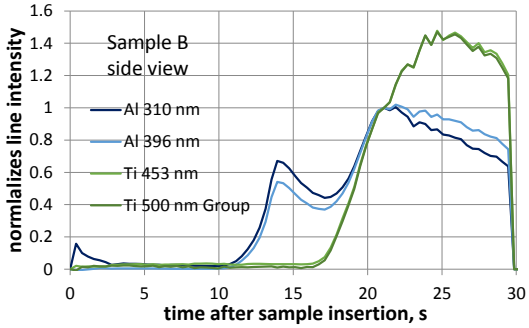

Figure 14. Line intensities of Al (310 and 396 nm) and Ti (453 nm and group around 500 nm) normalized to their value at 21 s in front of sample B vs. test time after sample insertion.

The final sample (sample C) was seeded with NaCl and $MgCl_2$ encapsulated in an epoxy disk of 0.88 mm thickness which was very similar to the samples tested in the mArc facility except using a disk shaped epoxy seed

rather than a rod. Fig. 13 shows FVB spectra for this sample in the side view with the Andor Shamrock spectrometer.

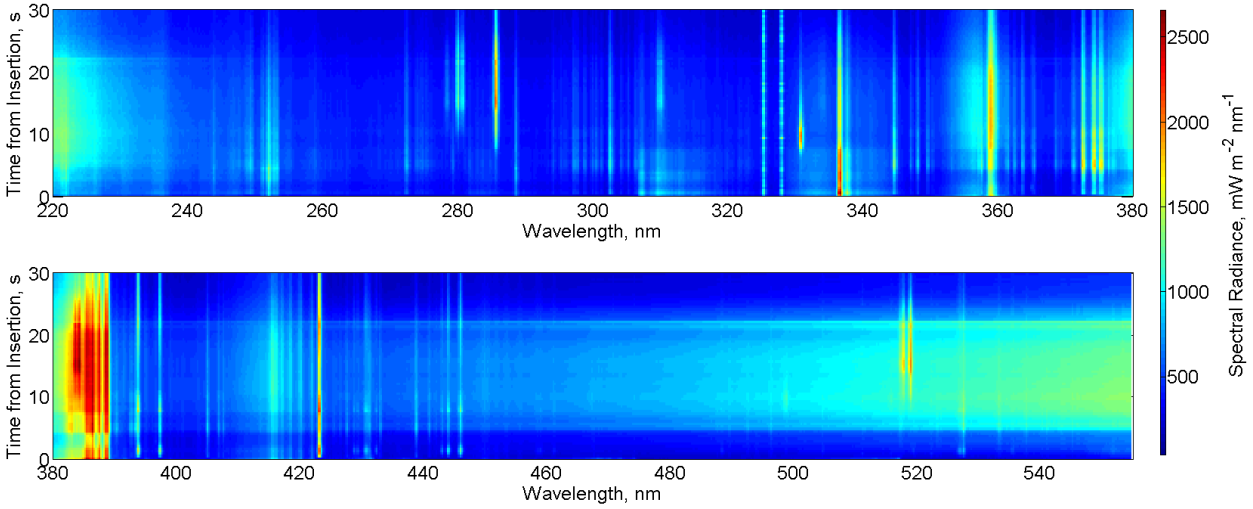

Figure 15. Time trace of integrated emission over the entire post-shock layer in front of sample C, seeded with NaCl and $MgCl_2$ encapsulated in an epoxy disk of 0.88 mm thickness.

As in the previous samples, strong emission of copper, CN, calcium and NH is seen. As in the mArc tests at NASA Ames,[5] no signs of chlorine are found in the spectra. The emission of sodium with the strongest lines in this spectral range at 330 and 495 nm and magnesium with lines at 280, 384 (strongly overlapping with CN emission), 517 and 518 nm are clearly seen with distinct temporal profiles.

The Na lines start showing up at 7 seconds after sample insertion, have a maximum at 10 s, and decay from there. The Mg lines start rising at about 7 s, peak at 16 s, but do not disappear entirely until the end of the test. Compared to samples A and B, the time the Mg lines appear in the spectrum agrees roughly with the time the V and Ti lines showed up, indicating that recession has reached the seeding depth. The Na lines, however, seem to leave the material with the pyrolysis gases. This disagrees with the results from earlier testing in the NASA Ames mArc facility where the Na and Mg lines showed the same time trace over test time. Furthermore, the emission of Mg (and to a lesser extend the one of Na) does not vanish completely from the spectra.

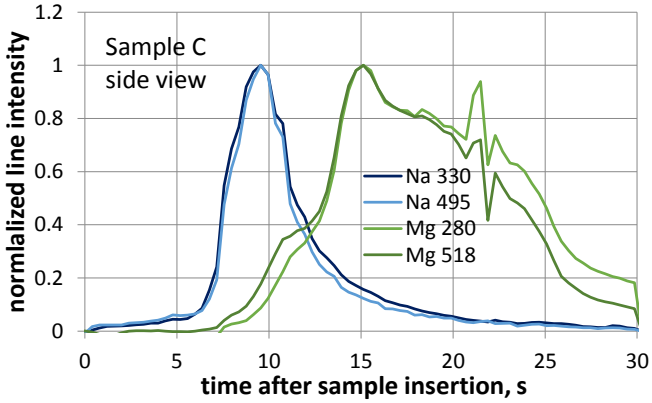

Figure 16. Line intensities of sodium (330 and 495 nm) and magnesium (280 and 518 nm) integrated over the entire post-shock layer in front of sample C vs. test time after sample insertion.

This might indicate some diffusion of seed material into the heat shield material. It is not entirely clear whether this might have happened during sample preparation or during the test itself. SEM investigations of the tested samples might give more information.

The line intensity time histories derived from the front view fiber-coupled miniaturized spectrometer as shown in Fig. 17 are in good agreement with the side view results. Na and Mg lines are clearly seen in the spectra although the lines at higher wavelengths are easier to distinguish than the UV lines.

However, recession appears to reach the seeded disk at about 20 s after insertion as seen in photos of the front surface of the sample shown in Fig. 18. After two more seconds, the seeded area is completely visible. During this time, sharp peaks in the Mg emission are visible in the line intensity time history indicating increased magnesium ablation once the seed material comes in contact with the plasma. In the photographs it appears, though, that most of the seed material has already disappeared and that a step is visible. Some of the magnesium has left the sample together with the pyrolysis gases as indicated by the Mg emission starting even before 10 s after sample insertion.

One hypothesis is that the epoxy used as a carrier pyrolyzes well before the recession reaches the seeding depth and carries both sodium and magnesium with it.

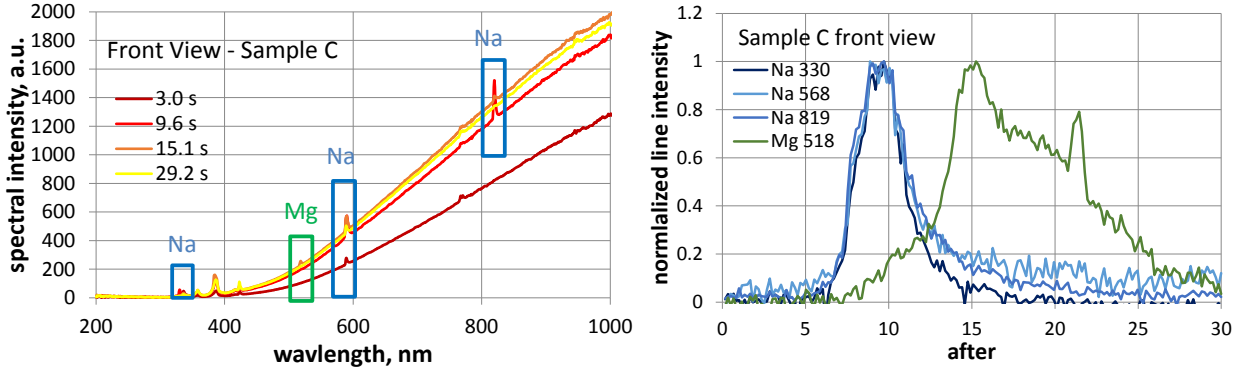

Figure 17. Front view spectra of sample C at 3, 10, 15, and 29 seconds after sample insertion and line intensities for sodium (330, 568, and 819 nm) and magnesium (518 nm).

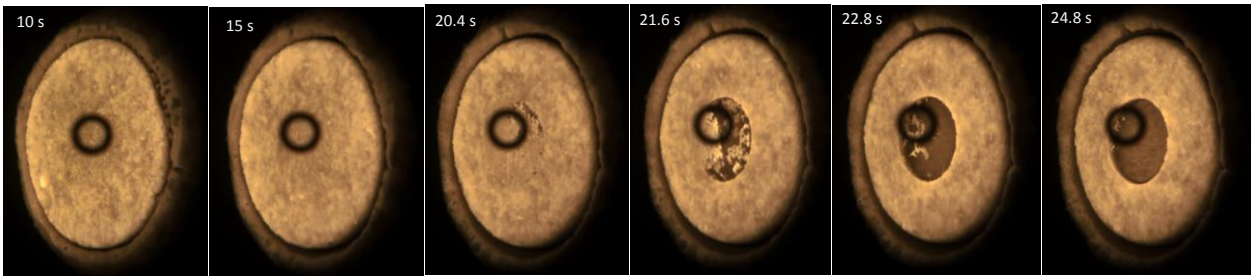

Figure 18. Front view of sample C at different times after sample insertion.

With the exception of Na, Mg, NaCl, and $MgCl_2$, all seed products show boiling temperatures higher than the measured sample surface temperature (which is assumed to be the highest temperature over the whole sample volume). In general, materials with lower melting points than the surface temperature of the sample seem to show up in the post shock emission before recession has reached the seeding depth. It is interesting, though that the time history of Al emission for samples A and B is nearly identical although sample A was directly seeded with aluminum with a low melting temperature of 933 K which could be reached in the pyrolysis zone while sample B was seeded with Al_2O_3 with a melting temperature of 2345 K very close to the surface temperature. It might be useful to repeat such tests with $MgCl_2$ and MgO which have drastically different melting temperatures but the same optical properties for the emitted radiation. Furthermore, the emission of titanium was clearly seen in the post-shock plasma although the seed material TiC has a higher melting temperature than the sample surface temperature. Table 6 illustrates the melting and boiling temperatures for the radiating elements and the original seed materials.

Table 6: Melting and boiling temperatures of seed materials and elements and approximate electronic excitation energies of transitions used in this work.

Material	T_{Melt}, K	$T_{Boiling}$, K	$E_{el\ exc}$, cm^{-1}	Material	$T_{Melting}$, K	$T_{Boiling}$, K
Na	370	1155	~ 17,000	$MgCl_2$	987	1685
Mg	923	1364	~35,000; ~41,000	NaCl	1074	1686
Al	933	2792	25,350; 34,435	Al_2O_3	2345	3250
Ti	1941	3560	20,000 - 25,000	VB_2	2373	
V	2183	3680	~26,000; ~32,000	MgO	3125	3873
Cu	1358	2835	~31,000	TiC	3433	5093

V. Summary and Conclusions

A method for remote recession measurements through emission spectroscopy measurements of the post shock layer radiation in front of a material sample in a plasma flow was studied experimentally. Different seed materials and different delivery methods were investigated. Processing investigations allowed the down-selection of Al_2O_3, HfO_2, VB_2 and Al as suitable candidates for seeding PICA samples. Two of those methods – infusing seed materials into a core of PICA and encapsulating seed material in an epoxy disk - were selected to produce material samples which were tested in the NASA Langley HYMETS arcjet facility at heating levels of 200 W/cm^2. The emission of the post shock layer was observed with a high resolution imaging spectrometer viewing the whole stagnation line from the side and with a fiber-coupled miniaturized spectrometer observing the sample surface in the wavelength range from 200 nm to 1,100 nm from the front through a collimator. The samples were encapsulated in a SiO_2 collar which was intended toprevent side wall heating but also forced the pyrolysis gases to leave through the sample front surface. Unfortunately, the collar material showed less recession than the PICA sample material therefore forming a rim which shaded the boundary layer close to the sample surface from observation through the side view spectrometer. Nevertheless, most of the seeded products were detected in the measured spectra. Seed elements with lower melting temperatures such as Na, Mg, and Al were seen in the post-shock emission spectra before the recession reached the actual seeding depth. One hypothesis is that they are carried with the pyrolysis gases and therefore not a clear sign for recession but for interactions with the pyrolysis gas at the seeding depth. This information could be useful in some applications, since it indicates the start of pyrolysis of the heat shield at that material depth. From photographs during the test it seems like the epoxy disk might have at least partly vanished before recession reached the seeding depth. The samples used here were not instrumented but if in-depth thermocouples would be used in future tests, it might be possible to assign defined pyrolysis zone temperatures to the emission of such seed materials. Seed materials with higher melting temperature such as V and Ti correlated nicely with the actual recession observed through a camera facing the sample front surface during insertion. Using NaCl and $MgCl_2$ as seed materials, a clear separation of the emission of Na and Mg was seen in time which was not observed during mArc testing of similar seed material. No explanation for this discrepancy has been found so far. It also remains to show whether materials which are border-line in terms of melting temperature compared to the sample surface temperature such as magnesium can be used as an indicator of recession if delivered in the form of a material with high melting point such as magnesium oxide.

Future testing of additional seed materials would be desirable. Certainly, measured temperature distributions inside the test sample, e.g. through in-depth thermocouples would be helpful with the interpretation of seed material with low melting/evaporation temperatures. However, for economic reasons and due to limited availability, the large NASA arcjet facilities used for TPS qualification testing are not suitable for such parametric studies. To prepare this promising technology for application in real re-entry missions, a parametrical investigation in ground test facilities in an academic environment is a more cost-effective way to achieve a Technology Readiness Level which makes this technology eligible for future NASA missions. Therefore, it is planned to continue the investigation of remote recession in the form of parametric studies in low power plasma facilities at the University of Kentucky.

Acknowledgments

The work on remote recession measurements and development of facilities and methods for the investigation of gas-surface interactions is supported by NASA Kentucky under NASA awards No: NNX10AL96H and No: NNX13AB12A, and by NASA Ames through the research grant NNX15AN74A. Financial support for the experimental work at NASA Langley was provided by NASA Kentucky EPSCoR Award NNX10AV39A. The authors would like to thank Michael Wright and Nagi Mansour from NASA Ames Research Center, Floyd Taylor and Herb Mefford at the University of Kentucky for their assistance in designing and machining many of the components necessary for this project, Zhaojin Diao and Helmut Koch for their help in preparing the measurement campaign, Gregory Gonzales, Joe Wang, Joel Seibert, and Joe Mach for their support at NASA Ames, and Jeff Gragg for his support and cooperation during testing at NASA Langley.

References

[1] Schairer, E. T., Heineck, J. T., "Photogrammetric recession measurements of ablative materials in arcjets," *Meas. Sci. Technol.*, 21 025304, 2010.

[2] Kontinos, D. A., Stackpoole, M., "Post-Flight Analysis of the Stardust Sample Return Capsule Earth Entry," AIAA 2008-1197, *46th Aerospace Sciences Meeting*, Reno, Jan. 2008

[3] Oishi, T., Martinez, E., "Development and Application of a TPS Ablation Sensor for Flight," *45th AIAA Aerospace Sciences Meeting and Exhibit*, 9-12 January 2008, Reno, NV.

[4] Trumble, K., Cozmuta, I., Sepka, S., Jenniskens, P., Winter, M., "Post-flight Aerothermal Analysis of the Stardust Sample Return Capsule,' *Journal of Spacecraft and Rockets*, Vol. 47, No. 5, pp. 765-764, Sept.-Oct. 2010.

[5] Winter, M. W., Stackpoole, M., Nawaz, A., Gonzales, G. L., Ho, T., "Remote Recession Sensing of Ablative Heat Shield Materials," *52nd AIAA Aerospace Sciences Meeting*, 13 - 17 January 2014, National Harbor, Maryland.

[6] Winter, M. W., McDaniel, R. D., Chen, Y-K., Liu, Y., Saunders, D., Jenniskens, P., "Radiation Modeling for the Reentry of the Hayabusa Sample Return Capsule," AIAA-2012-1296, *50th AIAA Aerospace Sciences Meeting*, Nashville, Tennessee, 9 - 12 Jan 2012.

[7] Splinter, S. C., Bey, K. S., Gragg, J. G., Brewer, A., "Comparative Measurements of Earth and Martian Entry Environments in the NASA Langley HYMETS Facility," AIAA Paper 2011-1014, *49th AIAA Aerospace Sciences Meeting*, January 4-7, 2011, Orlando, FL, 2011

[8] Johansen, C., Lincoln, D., Bathel, B., Inman, J., Danehy, P., "Simultaneous Laser-Induced Fluorescence of Nitric Oxide and Atomic Oxygen in the Hypersonic Materials Environment Test System Arcjet Facility," *17th International Symposium on Applications of Laser Techniques to Fluid Mechanics*, Lisbon, Portugal, 07-10 July, 2014.

[9] Lachaud, J., Mansour, N. N., Ceballos, A., Pejakovic, D., Zhang, L., Marschall, J.,"Validation of a volume-averaged fiber-scale model for the oxidation of a carbon-fiber perform," AIAA-2011-3640, *42nd AIAA Thermophysics Conference*, 27-30 June 2011, Honolulu, Hawaii.